

# 3D Simulation of Borosilicate Glass All-Electric Melting Furnaces

Hailong Li, Zhibin Xing, Shiqing Xu, and Shimin Liu<sup>†</sup>

State Key Laboratory of Metastable Materials Science and Technology, Yanshan University, Qinhuangdao 066004, China

Two all-electric melting furnaces, 15t/d and 36t/d, were simulated and analyzed with the ANSYS FLUENT 14.0 software add-on MHD module. The electric power density distribution, temperature distribution, and velocity field in the glass furnaces of these two models were analyzed. Electric power density and temperature are found to increase initially and then decrease from the center of the furnace to the side wall in a horizontal direction. Similar trend is observed from top to bottom in a vertical direction. The temperature distribution causes the internal and external circulations in the all-electric melting furnaces. An unstable connectivity relation is proven to exist between the external circulation flow and the dog-hole of the 15t/d all-electric melting furnace. Experimental evidence of the relation is presented from the annular strip images of the corresponding glass pipe product samples. Our analysis revealed several design flaws in the working condition of the two types of furnaces. The simulation results of the two models were compared.

## I. Introduction

COMPARED with soda-lime-silica float glass, borosilicate glass displays excellent performance in terms of thermal stability, chemical stability, mechanical behavior and mechanical properties, optical properties. Borosilicate glass has a broad market and can be utilized in a number of new areas with high added value. The production of borosilicate glass involves many technological difficulties owing to the high viscosity, high melting temperature, and volatility of boron and the phase separation of boron and silicon. An all-electric melting furnace can overcome these difficulties. Most borosilicate glass products (mainly tubular and rod-like) are produced by an all-electric melting furnace that maintains a qualified rate of 88% to 90%. Borosilicate glass products are influenced by the furnace shape, type of power supply, position and arrangement of the electrodes, and even the electrical conductivity of the molten glass. However, most researchers have scant knowledge on the electric power density distribution, temperature distribution, and velocity field in a furnace, which naturally arises the quality problems in the production of borosilicate glass. Therefore, electric heating regularity, glassmelting mechanism, and flow trend should be analyzed. It contributes greatly to large-scale electric-melting furnace design. Under the condition of guaranteeing the glass product quality, enlarge the all-electric melting furnace size is expected to improve the heat energy utilization in the process of glass manufacturing. This study helps enhance the quality of electric-molten glass products and improves the heat energy utilization in the all-electric melting furnace.

The studies of electric melting furnace simulation have been focused in some groups.

Austin and Bourne<sup>1</sup> published an article about two-dimensional simulation of an electric furnace. A two-dimensional mathematical model of glass electric melting was studied; the effects of different electrode configurations were discussed.

Choudhary<sup>2</sup> developed a three-dimensional mathematical model for calculating joule heat release, glass flow, and heat transfer in electric glass furnaces. The bulk glass temperature was found to be very uniform with large temperature gradients near the boundaries. The calculated flow pattern was, in general, quite complex with several circulation loops.

Giessler and Thess<sup>3</sup> presented a three-dimensional numerical study of glassmelt in a small-scale circular crucible heated by two rod electrodes. The results show that Lorentz forces provide a new approach to tuning the thermally driven convection of molten glass, leading to a possible improvement in mixing.

Bezuidenhout *et al.*<sup>4</sup> developed a complete three-dimensional computational fluid dynamic model to investigate the internal dynamics of a circular, three-phase electrical furnace used to smelt platinum group metal concentrates. The present model provides a foundation for future modeling investigations, which, when combined with rapid advancements in computing power, can improve understanding of the aggressive environment in electric smelting. However, further validation of the results is recommended to establish complete confidence in the outcome of the model.

Reynolds and Jones<sup>5</sup> examined a small twin-electrode DC arc furnace in their preliminary photographic study of the behavior of the two plasma arcs present in such furnaces. Results show that the arc trajectory follows a circular path, with the radius of curvature directly proportional to electrode separation and almost independent of electrical variables such as current.

The ANSYS FLUENT 14.0 software (ANSYS, Inc., Canonsburg, PA) was adopted in this study to simulate two borosilicate glass all-electric melting furnaces and examine electric power density distribution, temperature distribution, and velocity field. The characteristic rules of the complete molten state of the glass stream within the electric-melting furnaces were determined. The simulation results of the two models were compared. The causes of the product defects were also discussed to facilitate the development of an all-electric melting technology.

## II. Mathematical Modeling

### (1) Object of Study

A 15t/d all-electric melting furnace and 36t/d all-electric melting furnace, both operational, were utilized as research objects. Figure 1 presents a structural diagram of the 15t/d all-electric melting furnace. The melting region is shaped as a hexagon. The area of the melting end is 8.0 m<sup>2</sup>, and the depth is 2.2 m. This furnace utilizes a three-phase power supply. The shape of the electrodes is clubbed, and the material is molybdenum. All the electrodes are inserted into the glass furnace horizontally. The electrodes are installed in alternate surfaces with each surface having six electrodes. The diameter of the electrodes is 75 mm, and the section inserted into the glass furnace is 600 mm long.

J. Mauro—contributing editor

Manuscript No. 33034. Received April 13, 2013; approved August 7, 2013.

<sup>†</sup>Author to whom correspondence should be addressed. e-mail: qhd60m@126.com

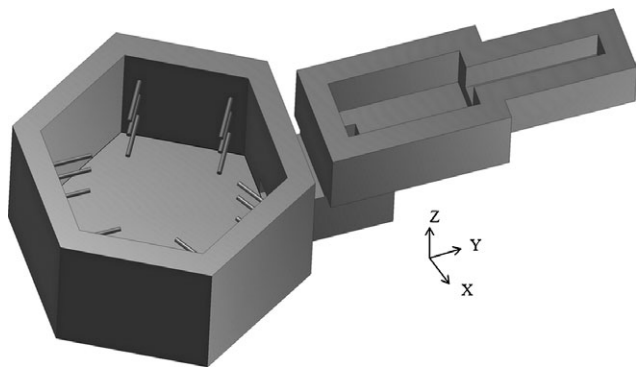


Fig. 1. Structural diagram of a 15t/d all-electric melting furnace.

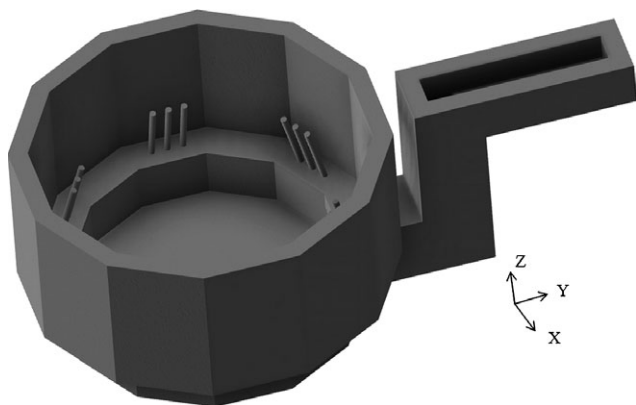


Fig. 2. Structural diagram of a 36t/d all-electric melting furnace.

Figure 2 presents a structural diagram of the 36t/d all-electric melting furnace. The melting region is shaped as a dodecagon. The horizontal cross-sectional area is 21.0 m<sup>2</sup> and the depth is 3 m. This furnace also utilizes a three-phase power supply. Clubbed molybdenum electrodes are obliquely inserted into the glass furnace. The electrodes are configured in alternate surfaces. The diameter of the electrodes is 100 mm, and the section inserted into the glass furnace is 1000 mm long.

The furnace width, length, and vertical directions are denoted as  $X$ ,  $Y$ , and  $Z$ , respectively, in these two types of furnaces.

## (2) Model Hypothesis

The simplified assumptions employed in the analysis are provided below.

1. The glass in the furnace is an incompressible Newtonian fluid, and the effects of the bubbles are ignored.
2. The effect of the cold batch (a phenomenon that keeps the batch surface cool) is ignored. The interface between the cold batch and glass furnace is set as the inlet velocity condition.
3. The influence of the refractory on the furnace wall is ignored and set as the radiating surface.
4. The refractory is insulated.
5. The effect of the material of the electrodes and cooling water jacket is ignored and considered an equipotential body.

## III. Boundary Conditions and Material Properties

### (1) Boundary Conditions

The boundary conditions are summarized in Table I.

Table I. Boundary Conditions of the Model

Yield (t/d)	$Y_{F1}$	15	$Y_{F2}$	36
Inlet velocity (m/s)	$v_{F1}$	$1.023 \times 10^{-5}$	$v_{F2}$	$0.965 \times 10^{-6}$
Inlet temperature (°C)	$T_{0F1}$	1450	$T_{0F2}$	1450
Outlet temperature (°C)	$T_{1F1}$	1250	$T_{1F2}$	1250
Outlet pressure	$P_{F1}$	0	$P_{F2}$	0
Wall thickness (m)	$t_{F1}$	0.3	$t_{F2}$	0.3
Thermal conductivity [ $W \cdot (m \cdot K)^{-1}$ ]	$\lambda_{F1}$	5	$\lambda_{F2}$	5
Free stream temperature (°C)	$T_{2F1}$	100	$T_{2F2}$	100
Voltage of the electrodes (V)	$U_{F1}$	$L_1$ 350 $L_2$ 350 $L_3$ 250	$U_{F2}$	250

F1 represents the 15t/d all-electrical melting furnace, and F2 represents the 36t/d all-electrical melting furnace.  $L_1$ ,  $L_2$ , and  $L_3$  represent the upper, middle, and lower layer electrodes of the 15t/d all-electrical melting furnace.

According to the hypothesis, the top surface of the melting end is considered as inlet. And on the basis of the volume of production and inlet area, the inlet velocity of the 15t/d all-electrical melting furnace is  $1.023 \times 10^{-5}$  m/s, and the 36t/d is  $0.965 \times 10^{-6}$  m/s. The velocity direction is downward. The initial temperature of the inflow molten glass is 1450°C.

Set the dog-hole as pressure-outlet, and the value is 0 Pa, the temperature is 1250°C.

The wall thickness is 0.3 m, the thermal conductivity is  $5 W \cdot (m \cdot K)^{-1}$ , and the free stream temperature is 100°C.

In the 15t/d all-electrical melting furnace, the voltages of upper, middle, and sub layer electrodes are 350, 350, and 250 V. In the 36t/d all-electrical melting furnace the voltage of electrodes is 350 V.

### (2) Material Properties

The glass composition is shown in Table II. It is the composition of the Pyrex glasses.

The thermophysical properties of the molten glass are summarized in Table III. The efficient thermal conductivity and specific heat of the melt are constant, whereas the density, viscosity, and electric conductivity of the melt are strongly dependent on temperature.

The efficient thermal conductivity and specific heat are calculated out by the commercial software Glass Engineer System. The Software programming based on lots references, main Refs. [6–8].

Viscosity is calculated by the formula<sup>6–8</sup>

$$\text{Lg}(\eta) = A + B/(T - T_0) \quad (1)$$

where  $\eta$  is viscosity,  $T_0$  is constant,  $A$  and  $B$  are based on the glass composition, and  $T$  is the temperature of the molten glass.  $A$  and  $B$  are also calculated out by the commercial software Glass Engineer System.

Electric conductivity is calculated by the formula<sup>9</sup>

$$\text{Lg}1/v = a + b/T \quad (2)$$

where  $v$  is electric conductivity,  $a$  and  $b$  are based on the glass composition, and  $T$  is the temperature of the molten glass. In this study  $a$  and  $b$  are fitting parameters from a resistivity-temperature curve from Ref. [9]. Which glass composition is: SiO<sub>2</sub> 80.5 wt%, Na<sub>2</sub>O 3.9 wt%, K<sub>2</sub>O 1.0 wt%, CaO 0.4 wt%, Al<sub>2</sub>O<sub>3</sub> 2.0 wt%, and B<sub>2</sub>O<sub>3</sub> 11.9 wt%.

Table II. The Glass Composition

Component	SiO <sub>2</sub>	Na <sub>2</sub> O	K <sub>2</sub> O	CaO	Al <sub>2</sub> O <sub>3</sub>	B <sub>2</sub> O <sub>3</sub>
Content (wt%)	78.9–82.1	3.8–4.0	0.9–1.1	0.3–0.5	1.9–2.1	11.6–12.1

Table III. Thermophysical Properties of the Molten Glass<sup>6–10</sup>

Physical property	Units	Value
Density	kg/m <sup>3</sup>	$\rho = 2474.4 - 0.20221T$
Efficient thermal conductivity	W·(m·K) <sup>-1</sup>	100
Viscosity	Pa·s	$Lg(\eta) = A + B/(T - T_0)$ $A = -4.4807, B = 6416.7631,$ $T_0 = 270.92$
Specific heat	J·(kg·K) <sup>-1</sup>	1006
Electric conductivity	S/m	$Lg1/\nu = a + b/T$ $a = 0.2546, b = 1288.3865$

According to Ref. [10], density can be calculated by the formula

$$\rho = 2474.4 - 0.20221T \quad (3)$$

where  $\rho$  is the density and  $T$  is the temperature of the molten glass. Its composition is: SiO<sub>2</sub>(78–90 wt%), B<sub>2</sub>O<sub>3</sub>(10–13 wt%), CaO(0–2 wt%), Al<sub>2</sub>O<sub>3</sub>(1–3 wt%), Na<sub>2</sub>O + K<sub>2</sub>O(5–10 wt%).

### (3) Numerical Solutions

Inventor (software) was utilized to create the glass furnace mathematical model. Gambit was employed to generate the mesh in which the inlet, outlet, wall, and other specific boundary types were defined. The FLUENT add-on turbulence and MHD modules were applied as solvers to define the material properties, boundary conditions, UDF (if necessary), and other parameters. The velocity and pressure terms were coupled by applying the SIMPLER algorithm in all the regions. The flow diagram of the simulation is shown in Fig. 3.

## IV. Simulation Results of the 15t/d all-Electric Melting Furnace

### (1) Electric Power Density Distribution

Electric power density is defined as the Joule heat generated by electrical energy in per unit volume and per unit time. Figure 4 shows the electric power density distribution in the different cross sections of the glass furnace. The color code represents the value logarithm of electric power density. Figures 4(a)–(d) present the horizontal cross sections at the upper, middle, and lower layers of the electrode center and above the dog-hole, respectively; Figs. 4(e) and (f) present the vertical cross sections at the furnace center along the Y axis and at the electrode center. The figures show that electric power density distribution is extremely uneven. Elec-

tric power density is highest at the tips of the middle layer electrodes at almost 10<sup>8</sup> W/m<sup>3</sup> and is reduced to 10<sup>6</sup> W/m<sup>3</sup> at the middle layer electrode root and to 10<sup>5</sup> W/m<sup>3</sup> at the sidewall. Electric power density is lowest at the center at 1 W/m<sup>3</sup>. The figures also show that electric power density declines sharply with the increase in the distance from the electrode tips. Electric power density is much lower at the central zone of the furnace than in the area near the electrodes.

Given that the distribution of electrodes is uneven, the electric field is not uniform. According to Joule's laws, electric power is proportional to the product of the conductor resistance and the square of the current. The resistance distribution of the glass becomes constant at stable working conditions. The Gauss theorem states that electric field lines diverge from the electrodes. The electric field line density near the electrodes is dense; electric current density is high; thus, electric power density is also high. The opposite is true in sections far from the electrodes.

### (2) Temperature Distribution

Figure 5 shows the temperature distribution in the different cross sections of the glass furnace. The color code represents the temperature values. The four different heights (1.6, 1.2, 0.5, and 0.3 m) of the horizontal cross sections along the furnace height direction are marked as (a), (b), (c), and (d). Figure 5 shows that the overall patterns of temperature distribution are similar. The temperatures at the electrode tips are the highest at 1587°C, 1648°C, 1629°C, and 1600°C. Temperature decreases gradually by increasing the distance from the electrodes. The isothermal curve is approximate to the annulus. Temperature increases initially and then decreases from the center to the sidewall because the electric power density near the electrodes is high in the horizontal direction, whereas electric power density is low at the center (far from the electrodes). The sidewall absorbs some heat and, thus, the temperature of the molten glass near the sidewall is low. As shown in Fig. 5, the maximum temperature differences in each cross section of (a), (b), (c), and (d) are 30°C, 80°C, 60°C, and 40°C, respectively.

Figures 5(e) and (f) present the vertical cross sections at the furnace center along the Y-axis and at the electrode center. The temperature increases initially and then decreases from top to bottom. The highest temperature (1648°C) is below the middle layer electrodes.

The glassmelting process in the furnace includes the decomposition of the silicate, the formation of molten glass, melt refining, homogenization, and cooling. The decomposition of the silicate and the formation of molten glass occur in the low-temperature zone. It is the process that batch heated up and melted into molten glass. During the process of the decomposition of the silicate a series of physical and chemical changes occurred, and main solid phase reaction is completed with a large number of gas escaping. Solids form molten glass as the temperature increases. There still exist a lot of bubbles and stripes, chemical composition and properties are not uniform. However, the mass of bubbles must be discharged in the melt refining process. The discharge of bubbles requires the glass to be low-viscosity; thus, it can be accomplished in a high-temperature zone near the hot spot. In this process the discharge of bubbles stir the molten glass and play a certain homogenization effect. Then it is the homogenization process. Due to the thermal motion of molten glass and mutual diffusion, stripe gradually disap-

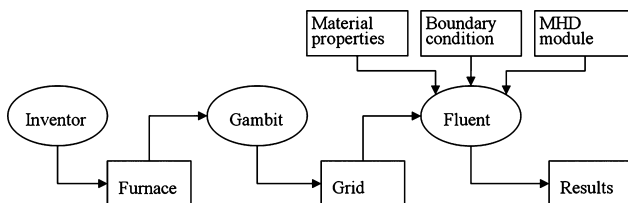
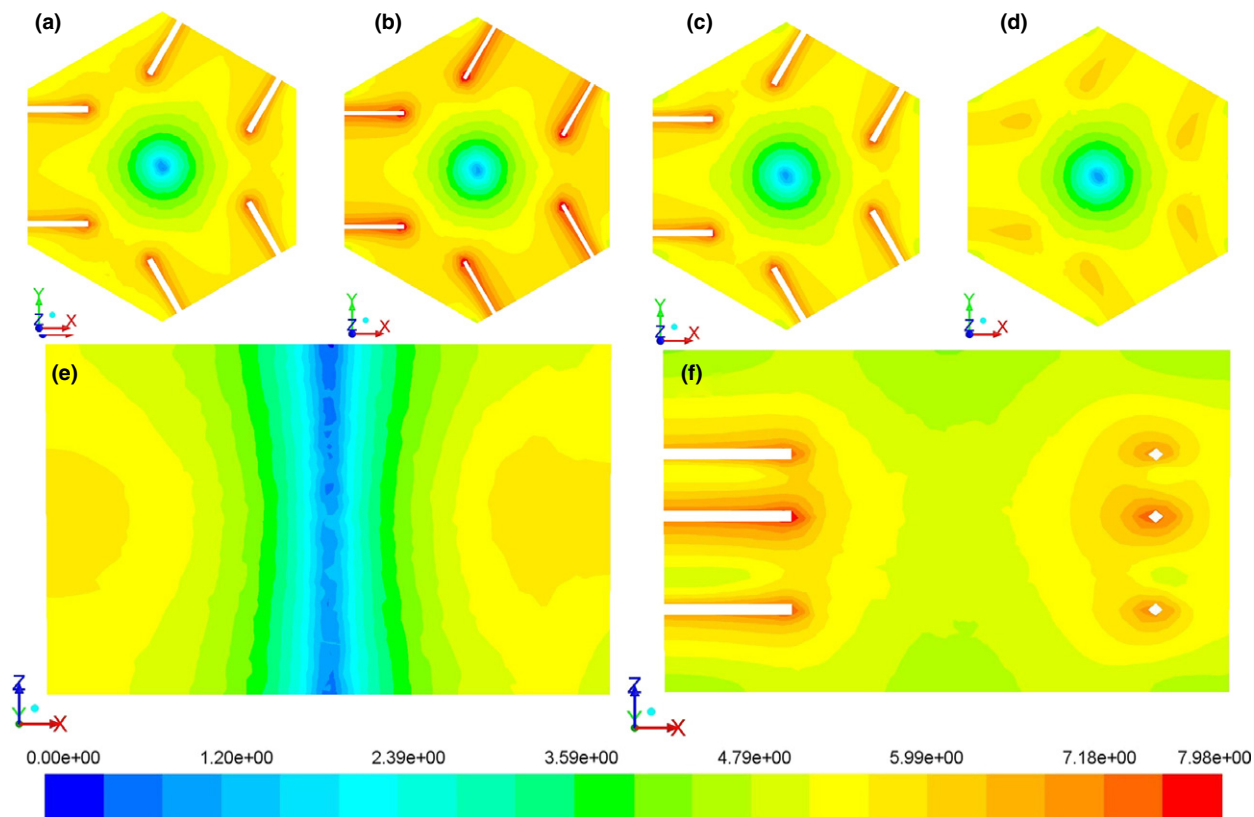
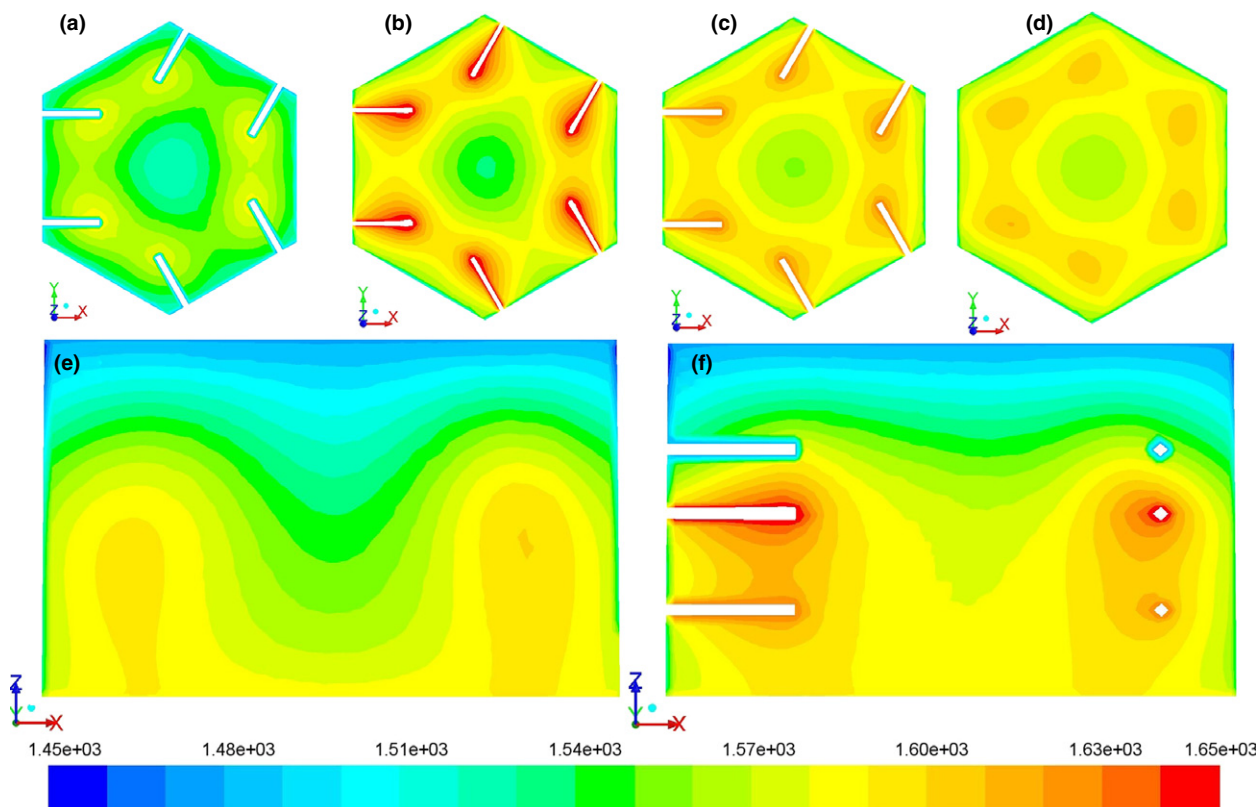


Fig. 3. Flow diagram of model solution.



**Fig. 4.** Nephogram of electric power density distribution in the different cross sections of the glass furnace. (a)  $z = 1.6$  m (upper layer electrode center); (b)  $z = 1.2$  m (middle layer electrode center); (c)  $z = 0.5$  m (lower layer electrode center); (d)  $z = 0.3$  m (above the dog-hole); (e)  $x = 0.875$  m (furnace center along the  $Y$  axis); and (f)  $x = 0.3$  m (electrode center).



**Fig. 5.** Nephogram of temperature distribution in the different cross sections of the glass furnace. (a)  $z = 1.6$  m (upper layer electrode center); (b)  $z = 1.2$  m (middle layer electrode center); (c)  $z = 0.5$  m (lower layer electrode center); (d)  $z = 0.3$  m (above the dog-hole); (e)  $x = 0.875$  m (furnace center along the  $Y$  axis); (f)  $x = 0.3$  m (electrode center). Unit:  $^{\circ}\text{C}$ .

peared, the chemical composition of glass and refractive index tend to be consistent. The glass flows out of the furnace during homogenization, and the temperature should be lower than that in the melt refining process. During glass melting, the temperature increases to reach the temperature of the melt refining process and then decreases to the temperature of the forming process. No flame heating occurs in the all-electric melting furnace; heat is directly generated from the electrodes through vertical melting technology. The simulation of temperature distribution along the height of the furnace is consistent with the actual situation.

### (3) Glass Velocity Field

Figure 6 shows the Z-axis velocity nephograms of the different cross sections of the glass furnace. Figures 6(a)–(d) show the horizontal cross sections in the upper, middle, and lower layer electrode center and above the dog-hole. Figures 6(e) and (f) show the vertical cross sections at the furnace center along the Y-axis and at the electrode center. The color code represents the velocity value. The black lines in these figures are the zero lines. The negative value represents the downward flow, and the positive value represents the upward flow. As shown in Figs. 6(a)–(d), the glass near the sidewall and at the central zone exhibit a downward flow, whereas that near the electrodes exhibits an upward flow.

Figure 7 presents a vector diagram of the center section along the length of the furnace. Two primary circulation flows occur in the glass furnace. The left one flows clockwise, and the right one flows counterclockwise. The two circulation flows intersect in the furnace center in a vertical direction. The circulation flow consisting of an upward flow near the electrodes and a downward flow in the central zone is defined as the interior circulation flow in this study. The circulation flow consisting of an upward flow near the electrodes and a downward flow near the sidewall is defined as the exterior

circulation flow. The simulation results reveal that the maximum velocity of the upward flow is  $4.56 \times 10^{-3}$  m/s, which is 400 times faster than the inlet velocity. The maximum velocity of the downward flow is  $6.89 \times 10^{-3}$  m/s, which is 600 times faster than the inlet velocity. The all-electric melting furnace has strong convections, and the main component is the interior circulation flow.

The circulation flows in the all-electric melting furnace are mainly caused by the temperature gradient. The density gradient is attributed to the temperature gradient owing to thermal expansion. The low-density (high temperature) glass moves upward and the high-density (low temperature) glass moves downward because of gravity. Analysis indicates that temperature is low at the central zone and sidewall and high near the electrodes, thereby producing the two circulation flows.

The operating condition of the circulation flows is different along the length of the furnace. One side of the furnace is linked to the dog-hole. The circulation flows were divided into four parts from the head to the end of the furnace) in this study. The parts were marked as I, II, III, and IV. Circulation flows I and IV are exterior circulation flows, and circulation flows II and III are interior circulation flows (Fig. 8).

### (4) The Coupling Between Electric Power Density Distribution, Temperature Distribution and Velocity Field

The normal operation of a furnace is the result of interactions between the fields. Because of the velocity field, low temperature molten glass that formed by the new batch flow down from the center of glass furnace. This is another reason that temperature at the center is lower than that near the electrodes. Glass absorbs heat and temperature gradually increases as it flows down. Part of glass flows out from the dog-hole directly and takes away some heat, while other part

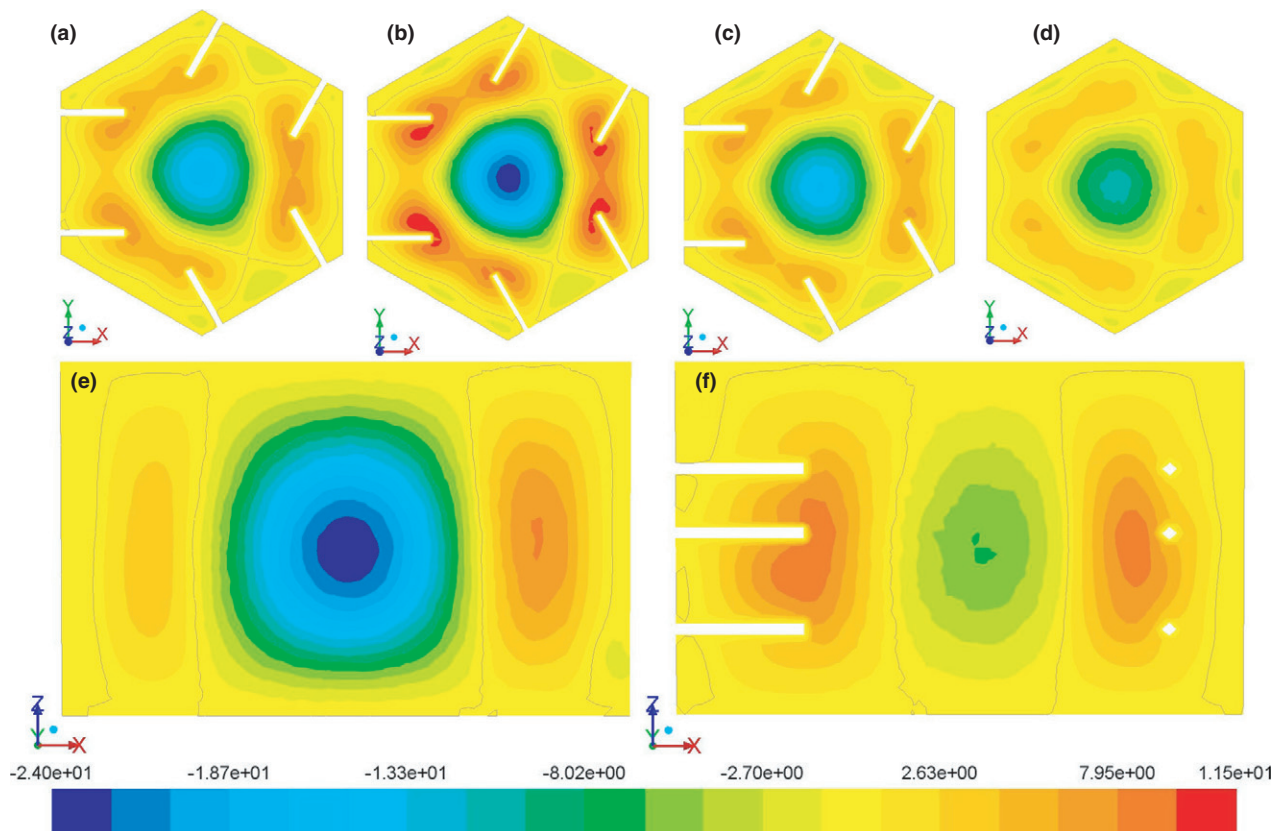


**Fig. 6.** Nephogram of Z-axis velocity in the different cross sections of the glass furnace. (a)  $z = 1.6$  m (upper layer electrode center); (b)  $z = 1.2$  m (middle layer electrode center); (c)  $z = 0.5$  m (lower layer electrode center); (d)  $z = 0.3$  m (above the dog-hole); (e)  $x = 0.875$  m (furnace center along the Y-axis); and (f)  $x = 0.3$  m (electrode center). Unit: m/h.

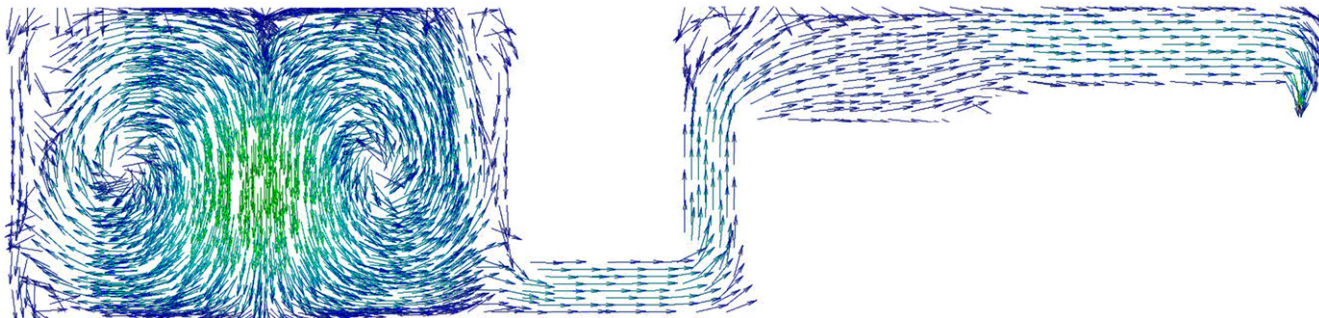


Fig. 7. Velocity vector diagram of  $x = 0.875$  m (furnace center) section.

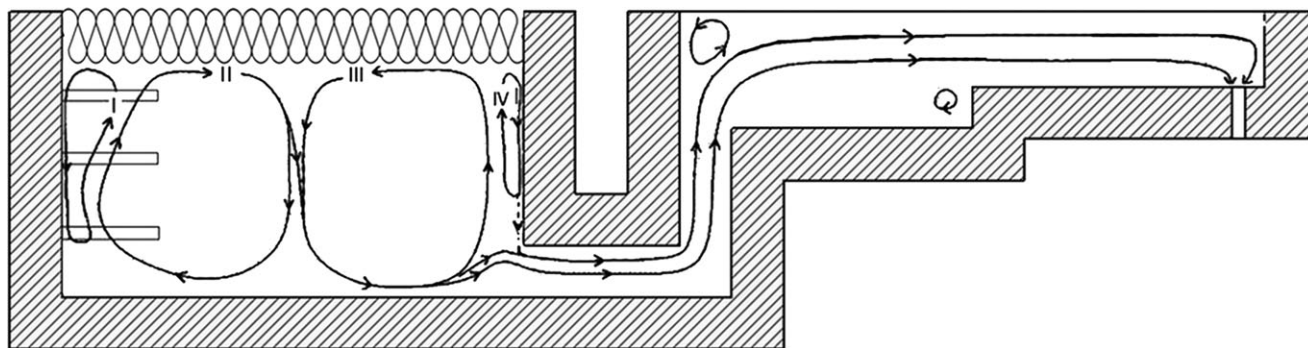


Fig. 8. Glass furnace flow diagram of the 15t/d all-electric melting furnace.

mixes with the circulation flow. In the process of circulation, the glass temperature rises when close to the electrodes. Some of the heat radiate to the low temperature glass, and some of the heat is taken away by circular glass and transfer to the glass at low temperature. It is because the interact balances of the velocity field and temperature distribution that glass furnace can operate stably.

There is no direct relationship between electric power density distribution and velocity field; they are indirectly influenced by temperature distribution. Electric power density distribution influences temperature distribution, and the molten glass density change with the temperature, in turn, affects velocity field. Velocity field influences temperature distribution, and the electrical conductivity is directly affected by temperature, in turn, affects electric power density distribution. Therefore, to have a reasonable temperature distribution and velocity field, it is significant to arrange the electrodes reasonably and get an ideal electrical power density distribution.

## V. Simulation Results of the 36t/d all-Electric Furnace

### (1) Electric Power Density Distribution

Figure 9 shows the electric power density distribution in the different horizontal and vertical cross sections (center sections along the furnace length and electrode center) of the glass furnace. The color code represents the logarithm value of electric power density. The electric power density distribution in the glass furnace is similar to that of the all-electric melting furnace with horizontally inserted electrodes. Compared with horizontally inserted electrodes, obliquely inserted electrodes are much closer to the sidewall, causing a marked increase in electric power density. At sidewall the electric power density is approximately  $10^6$  W/m<sup>3</sup>. Considering that the central zone is located far from the electrodes, the electric power density is low (approximately 1 W/m<sup>3</sup>). The electrodes are obliquely inserted into the glass furnace. The electrode distribution is relatively uniform, thus

producing a relatively uniform electric power density distribution.

### (2) Temperature Distribution

Figure 10 shows the temperature distribution in the different cross sections of the glass furnace. The color code represents the temperature values. Figures 10(a)–(d) show the four horizontal cross sections along the height of the furnace. The height distances are 2.4, 2.0, 1.5, and 0.8 m. The temperature distributions are similar to those in the 15t/d all-electric melting furnace. The temperature at the electrode tips is highest at 1620°C and gradually decreases with the increase in the distance from the electrodes. The temperature increases and then decreases from the center to the sidewall. Compared with the 15t/d all-electric melting furnace, the maximum temperature differences in each cross section of the 36t/d all-electric melting furnace are lower at 15°C, 50°C, 45°C, and 20°C.

Figures 10(e) and (f) present the vertical cross sections at the furnace center along the  $Y$ -axis and at the electrode center. The temperature distributions are similar to those in the 15t/d all-electric melting furnace. The temperature increases initially and then decreases from top to bottom along the vertical direction. However, the temperature exhibits an almost layered distribution.

Temperature distribution is influenced by electric power density distribution. And because the electrodes are inserted obliquely, the electric power density near the sidewall increases, thus the temperature there also increases. The dodecagon shape of the 36t/d all-electric melting furnace structure addresses the dead corner problem and increases the temperature near the sidewall; therefore, the maximum temperature difference in the horizontal cross sections is reduced. The electrode distribution and electric field line are uniform in the vertical direction. Thus, the complexity of temperature is reduced and the layered temperature distribution becomes obvious.

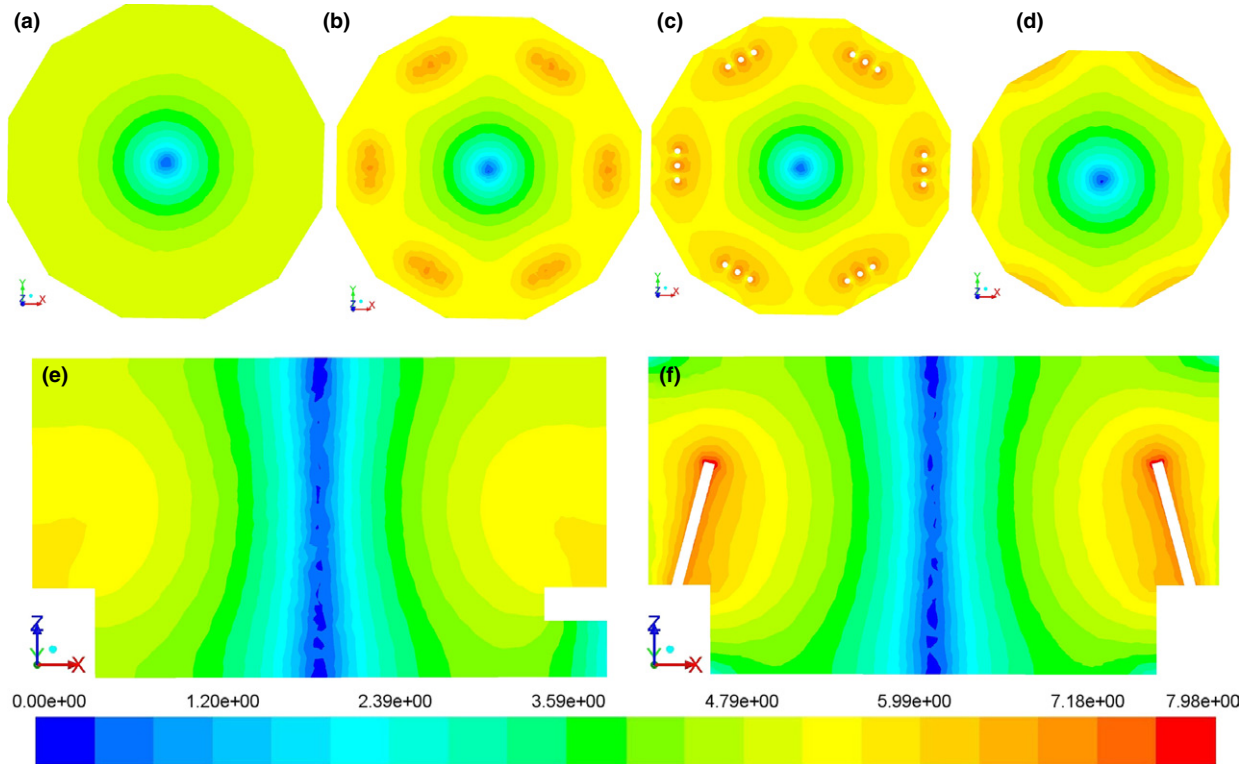


Fig. 9. Nephogram of electric power density distribution in the different cross sections of the glass furnace. (a)  $z = 2.4$  m; (b)  $z = 2.0$  m; (c)  $z = 1.5$  m; (d)  $z = 0.8$  m (above the contraction section); (e)  $x = 2.56$  m (furnace center along the  $Y$ -axis); (f)  $x = 2.56$  m (electrode center).

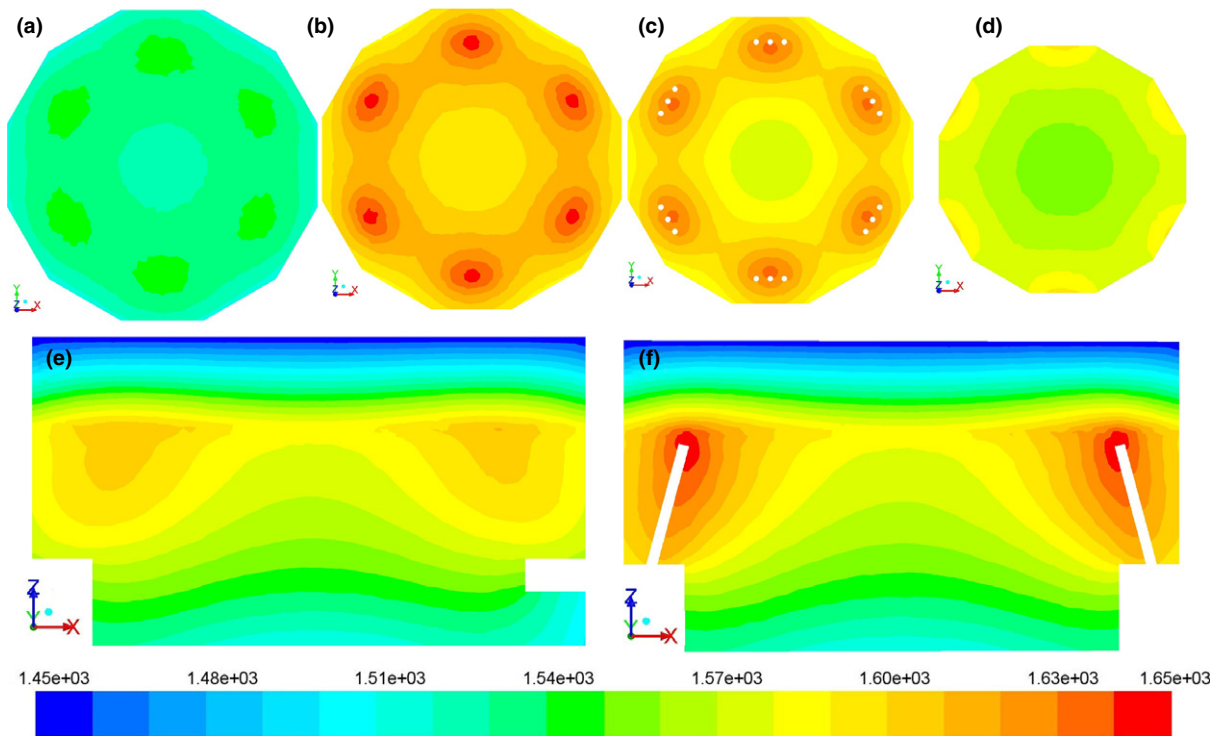
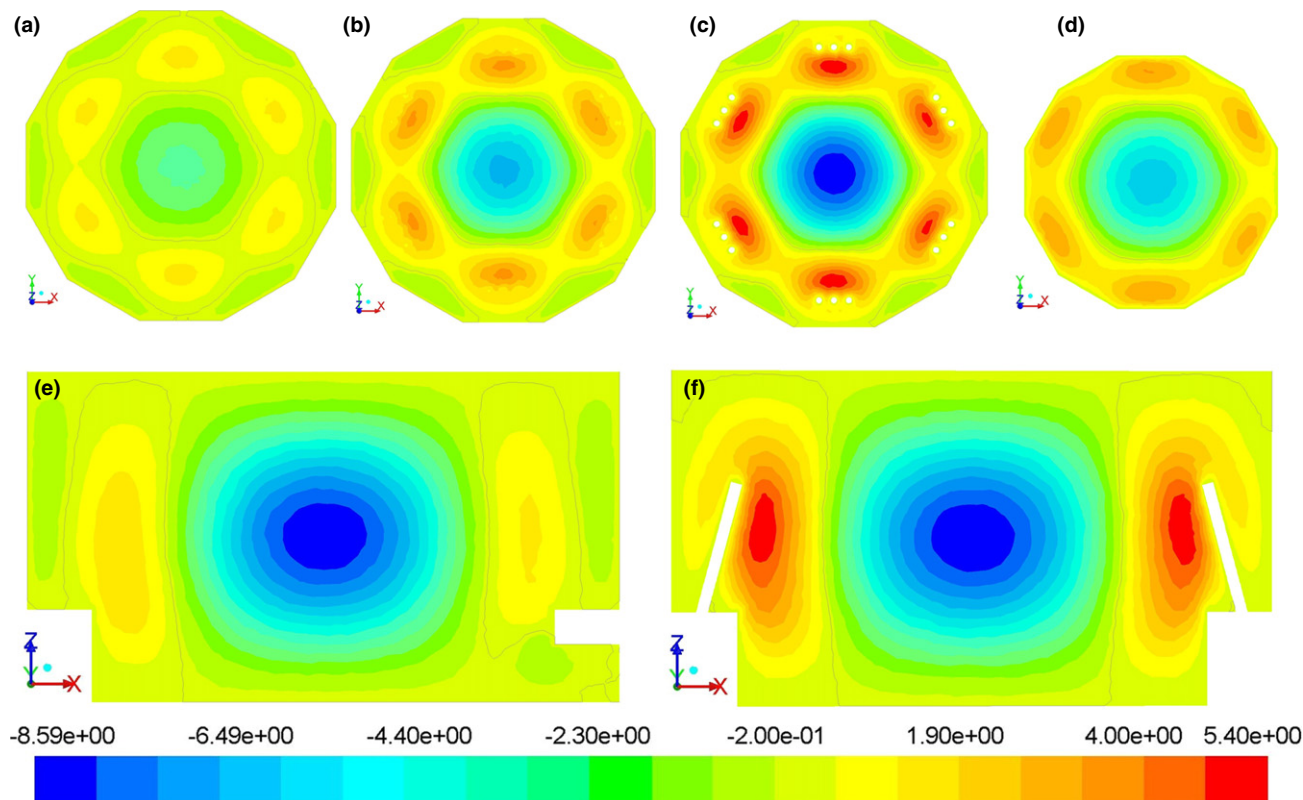


Fig. 10. Nephogram of temperature distribution in the different cross sections of the glass furnace. (a)  $z = 2.4$  m; (b)  $z = 2.0$  m; (c)  $z = 1.5$  m; (d)  $z = 0.8$  m (above the contraction section); (e)  $x = 2.56$  m (furnace center along the  $Y$ -axis); and (f)  $x = 2.56$  m (electrode center). Unit:  $^{\circ}\text{C}$ .

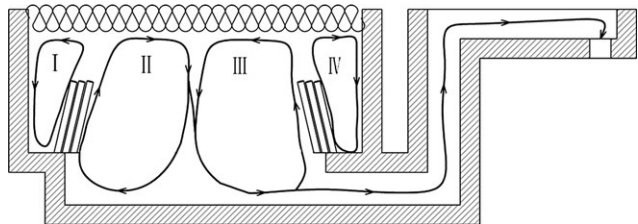
**(3) Glass Velocity Field**

Figure 11 shows the  $Z$ -axis velocity nephogram of the different cross sections of the melting end. The color code represents the velocity values. The black lines in the figures are the zero lines. The negative value indicates a downward velocity direction, and the positive value indicates an upward

velocity direction. Figures 11(a)–(d) show the four horizontal cross sections along the height of the furnace with the height distance of 2.4, 2.0, 1.5, and 0.8 m, respectively. The glass furnace exhibits a downward flow near the sidewall and central zone, whereas an upward flow is exhibited near the electrodes. Similar to the 15t/d all-electric melting furnace, the



**Fig. 11.** Nephogram of velocity in the different cross sections of the glass furnace. (a)  $z = 2.4$  m; (b)  $z = 2.0$  m; (c)  $z = 1.5$  m; (d)  $z = 0.8$  m (above the contraction section); (e)  $x = 2.56$  m (furnace center along the  $Y$ -axis); and (f)  $x = 2.56$  m (electrode center). Unit: m/h.



**Fig. 12.** Glass furnace flow diagram of the 36t/d all-electric melting furnace.

36t/d furnace also has two circulation flows. Figure 12 shows that the circulation flows were divided into four parts from the head to the end of the furnace; the parts are marked as I, II, III, and IV. Figures 10(e) and (f) present the vertical cross sections. A downward flow occurs near the sidewall. However, the contraction section above the dog-hole separates downward flow IV from the dog-hole. In this case, the incompletely melted mixtures or corroded refractory materials are prevented from flowing directly into the dog-hole and adversely affecting the quality of the glass products.

The coupling between electric power density distribution, temperature distribution, and velocity field is described in section 4.4.

## VI. Comparison and Analysis

### (1) Comparison of the Physical Field Distributions

Electrode distribution and insertion mode cause electric power density distribution to be uneven. The comparison of the two furnaces reveals several electric power density distribution characteristics. At the sidewall and central zone, the electric power density is much lower than that around the electrodes. In the horizontal direction, the electric power density increases and then decreases from the center to the

sidewall. In the vertical direction, it increases and then decreases from top to bottom.

The same characteristics are observed for temperature distribution and velocity field. In the horizontal direction, the temperature increases initially and then decreases from the center to the sidewall. In the vertical direction, it increases and then decreases from top to bottom. The hot spot is located at the furnace center and near the electrodes; however, the height of the hot spot differs in the two furnaces.

The internal temperature gradient in the glass furnace greatly influences the velocity field. The temperature distribution characteristic in the horizontal direction causes the interior and exterior circulation flows. The circulation flows were divided into four parts (I, II, III, and IV) from the head to the end of the furnace in the middle cross section. Circulation flows I and IV are exterior circulation flows, whereas circulation flows II and III are interior circulation flows.

The physical simulation of the all-electric furnace by Stanek<sup>11</sup> shows that interior and exterior circulation flows exist in the all-electric melting furnace. The results of Stanek's study concur with our simulation results.

### (2) Glass Homogeneity Analysis

Figure 13 presents a schematic of the tube glass production process in the 15t/d all-electric melting furnace. The molten glass from the melting furnace flows into the feeder bowl and overflows to form tubular glass products. The physical map of the glass sample provides a graphical direction for tubular glass girdling. Figure 14 presents the annular strip images of the glass pipe product samples from different production batches. Figure 14(a) presents an annular strip image of the glass pipe product sample from an acceptable production batch. The strip stratification phenomenon in this figure is obvious and basically cricoid the distribution. The same phenomenon was observed in the simulation results, indicating

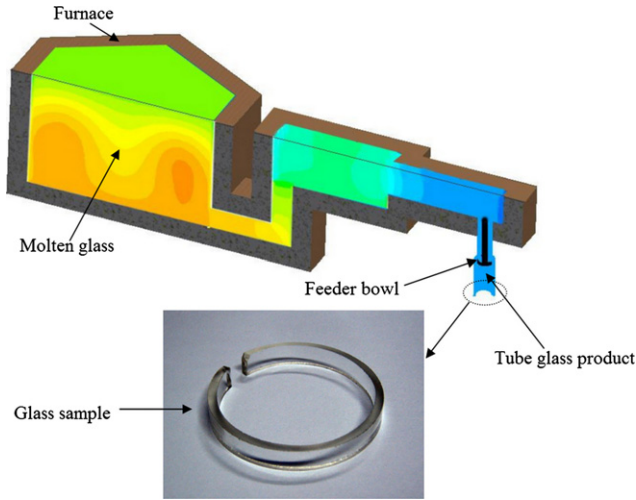


Fig. 13. Schematic of the tube glass production process.

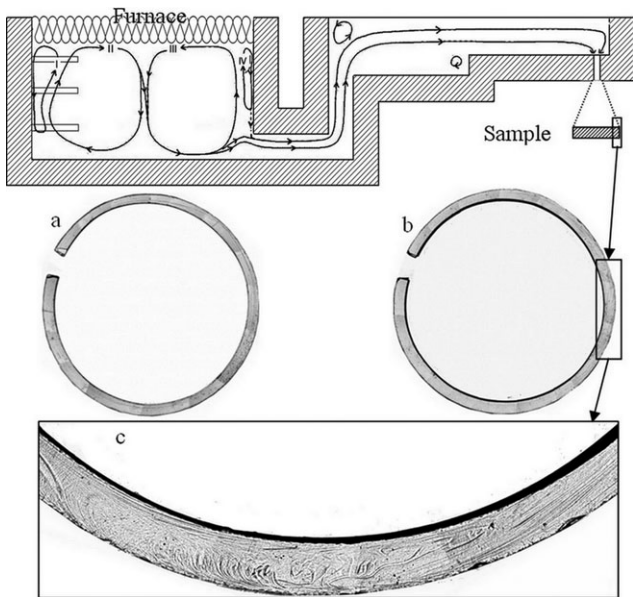


Fig. 14. Ring-cutting striped images of the glass pipe product samples from different production batches. (a) Qualified sample, (b) inferior-quality sample, and (c) partially enlarged view.

that interior and exterior circulation flows exist in the all-electric melting furnace. Figure 14(b) presents an annular strip image of an inferior-quality glass pipe product sample, and Fig. 14(c) presents a partially enlarged view of the same sample. The glass stripes are complicated and exhibit poor homogeneity. This part of the stripe originated from circulation flow IV in the glass fluid, which caused the incompletely melted mixtures or corroded refractory materials to flow directly out of the dog-hole. Such phenomenon was not observed in Fig. 14(a) in the working condition. A possible reason for this is that circulation flow IV in the same working condition did not connect with the dog-hole. The occurrence of this phenomenon clearly depends on the working condition.

A contraction section is set at the bottom of the 36t/d all-electric melting furnace. This section separates downward circulation flow IV and the dog-hole and effectively prevents the incompletely melted mixtures or corroded refractory materials from flowing directly into the dog-hole, thereby ensuring the high quality of the glass products.

## VII. Conclusions

Two borosilicate glass all-electric melting furnaces, namely, 15t/d and 36t/d, were analyzed through the ANSYS FLU-ENT 14.0 software add-on MHD module. Electric power density distribution, temperature distribution, and glass velocity field were analyzed through simulation, and the results were confirmed by the strip images. Below are the conclusions obtained from this study.

1. The patterns of electric power density and temperature distribution exhibited by the two all-electric melting furnaces are as follows: electric power density and temperature are found to increase initially and then decrease from the center to the sidewall in a horizontal direction; and electric power density and temperature increase and then decrease from top to bottom in a vertical direction. The hot spot of the 15t/d all-electric melting furnace is located near the tips of the middle layer electrodes. The temperature in the hot spot is 1648°C. The maximum temperature difference in the horizontal section is 80°C. The hot spot of the 36t/d all-electric melting furnace is located near the tips of the electrodes. The temperature in the hot spot is 1620°C. The maximum temperature difference in the horizontal section is 50°C.
2. Both furnaces have an interior and exterior circulation flow owing to the influence of electric power density and temperature distribution. The circulation flows are divided into four parts from the head to the end of the furnace in the middle cross section. The parts are marked as circulation flow I, II, III, and IV. Circulation flows I and IV are exterior circulation flows, whereas circulation flows II and III are interior circulation flows.
3. The simulation results and sampling results show that in the 15t/d all-electric melting furnace, circulation flow IV could cause the incompletely melted mixtures or corroded refractory materials to flow directly into the dog-hole. In the 36t/d all-electric melting furnace, the contraction section above the dog-hole can prevent the occurrence of the above-mentioned phenomenon. Thus, a contraction section should be set above the dog-hole in all-electric melting furnace.

## References

- <sup>1</sup>M. J. Austin and D. E. Bourne, "A Mathematical Model of an Electric Glass Furnace," *Glass Technol.*, **14** [3] 78–84 (1973).
- <sup>2</sup>M. Choudary, "A Three Dimensional Mathematical Model for Flow and Heat Transfer in Electric Glass Furnaces," *Industry and General Applications*, **23** [5] 912–21 (1986).
- <sup>3</sup>C. Giessler and A. Thess, "Numerical Simulation of Electromagnetically Controlled Thermal Convection of Glass Melt in a Crucible," *Int. J. Heat Mass Transf.*, **52** [16] 3373–89 (2009).
- <sup>4</sup>J. J. Bezuidenhout, J. J. Eksteen, and S. M. Bradshaw, "Computational Fluid Dynamic Modelling of an Electric Furnace Used in the Smelting of PGM Containing Concentrates," *Miner. Eng.*, **22** [11] 995–1006 (2009).
- <sup>5</sup>Q. G. Reynolds and R. T. Jones, "Twin-Electrode DC Smelting Furnaces—Theory and Photographic Testwork," *Miner. Eng.*, **19** [8] 325–33 (2006).
- <sup>6</sup>A. Fluegel, "Global Model for Calculating Room-Temperature Glass Density From the Composition," *J. Am. Ceram. Soc.*, **90** [8] 2622–5 (2007).
- <sup>7</sup>A. Fluegel, D. A. Earl, A. K. Varshneya, and T. P. Seward III, "Density and Thermal Expansion Calculation of Silicate Glass Melts From 1000°C to 1400°C," *Phys. Chem. Glasses: Eur. J. Glass Sci. Technol. B*, **49** [5] 245–57 (2008).
- <sup>8</sup>F. Gan, *Calculation of Physical Properties of Inorganic Glasses and Component Design*, (in Chinese). Shanghai Science and Technology Press, Shanghai, 1981.
- <sup>9</sup>J. Chen, *Glass Electric Melting Furnace Technology*, (in Chinese). 3–8, Chemical Industry Press, Beijing, 2007.
- <sup>10</sup>P. Lu, *The Research of Thermal Shock Borosilicate Glass Float Forming Process*, (in Chinese). Wuhan University of Technology, Wuhan, 2008.
- <sup>11</sup>J. Staněk and J. Matěj, "Electric Melting of Glass," *J. Non-Cryst. Solids*, **84**[1–3]353–62(1986). □